# Smart Material Composites for Discrete Stiffness Materials

# Emily A Allen, Lee D Taylor and John P Swensen

School of Mechanical and Materials Engineering, Washington State University, 355 NE Spokane St, Pullman, WA 99163

E-mail: emily.allen2@wsu.edu, lee.taylor@wsu.edu, john.swensen@wsu.edu

**Abstract.** This paper presents an initial step towards a new class of soft robotics materials, where localized, geometric patterning of smart materials can exhibit discrete levels of stiffness through combinations of smart materials. This work is inspired by a variety of biological systems where actuation is accomplished by modulating the local stiffness in conjunction with muscle contractions. Whereas most biological systems use hydrostatic mechanisms to achieve stiffness variability, and many robotic systems have mimicked this mechanism, this work aims to use smart materials to achieve this stiffness variability. Here we present the compositing of the low melting point Field's metal, shape memory alloy Nitinol, and a low melting point thermoplastic Polycaprolactone (PCL), composited in simple beam structure encased in silicone rubber. A simple two-joint soft robotic finger is constructed to demonstrate the dexterous capabilities of smart composite materials. The comparison in bending stiffnesses at different temperatures, which reside between the activation temperatures of the composited smart materials demonstrates the ability to achieve discrete levels of stiffnesses within the soft robotic tissue.

Keywords: smart materials, shape memory alloys, soft robotics, multi-stiffness materials, stiffness variability, biomimetic

Submitted to: Smart Mater. Struct.

### 1. Introduction

Soft robotics and compliant robotic mechanisms have gained increasing popularity in the past decade within the academic community. This soft robotics approach is in stark contrast to the traditional paradigm of large, heavy, rapidly-moving robotics in isolated environments. The soft-robotic approach has shown promise because their compliant nature lends itself well to safety concerns in co-robotics environments and exhibits adaptability and robustness to uncertainty, such as in robotic grasping. However, this same intrinsic compliance in soft robotics is also its greatest drawback—in many scenarios it is unable to exert necessary forces and control manipulator shape under external loading.

However, biological systems abound where the primary method of actuation is the ability to adjust the stiffness of tissues in conjunction with localized muscle contractions. These type of actuation methods are widely prevalent in the muscular hydrostats, catch muscles, and catch connective tissues in cephalopods and echinoderms [1, 2]. This combination of colocated muscle and adaptive tissue provide these animals with the ability to squeeze through holes much smaller than their average body diameter and capture or crush their prey. The primary focus of this paper is the development of new techniques in the compositing of existing soft-robotic technologies and carefully designed geometry of smart material additives to create robotic components with the ability to switch between acting as soft robotics or traditional rigid robotics, approaching the extreme capabilities of their biological counterparts, by presenting multiple discrete levels of stiffness.

Traditionally, robotic systems have followed the paradigm of being comprised primarily of rigid structures with relatively few degrees of freedom and well-characterized motion driven by actuators directly connected to the rigid links. In recent years, there has been an explosion of research in the area of soft robotics, as they provide the promise of allowing robots and humans to work and collaborate in the same workspace. Additionally, soft robotics has proven to be an ideal testbed for taking inspiration from biological systems, as described above, and including them in soft robotic designs that exhibit either bio-mimicry or bio-inspiration [3, 4, 5, 6]. However, soft robotics have inherently limited ability to exert forces and interact

with their surroundings in a meaningful way because of their compliant nature. Hence there is a great need for materials and mechanisms that have the ability to dynamically change between acting as a soft or a rigid robotic component.

# 1.1. Variable stiffness actuators

Many variable stiffness actuators require complex design and machining to achieve a change of stiffness in even a single degree of freedom [7, 8, 9]. These often involve a high degree of complexity in terms of motors, mechanisms, and/or cable routings. Other approaches require high bandwidth feedback control to render a variable stiffness through a control system [10, 11]. These approaches are usually not scalable and are more targeted at applications with a distinct drive train, rather than as material actuators and structures. However, when amenable these approaches provide the highest fidelity of rendered variable stiffness.

# 1.2. Variable stiffness structures

Tensile integrity, or tensegrity, structures were initially used in architecture and artwork, with the term coined by Buckminster Fuller. It is characterized by systems of struts and cables where all of the cables have been prestressed and struts are either in compression or tension, thus maintaining the structural integrity of the whole. When applied to robotic systems, these tensegrity structures are designed such that the robot can selectively release tension in one or more cables, resulting in a predictable motion during collapse. Sequential loading and unloading of the cable generates reproducible gaits [12, 13]. Other researchers are focusing on the valid tensegrity configurations that result in predictable deformations and their associated control [14, 15].

# 1.3. Soft Robotic Actuators

The majority of soft robotics, both actuators and systems, are primarily concerned with the problem of compliance matching to the task of the robotic system [16]. This is often accomplished through fabrication using purely elastomeric materials or with geometrically-complex chambers and pneumatic controls to deform an elastomer when the chambers are pressurized [17, 18, 19]. Previously, other geometric approaches to compliance were dominated by tendon

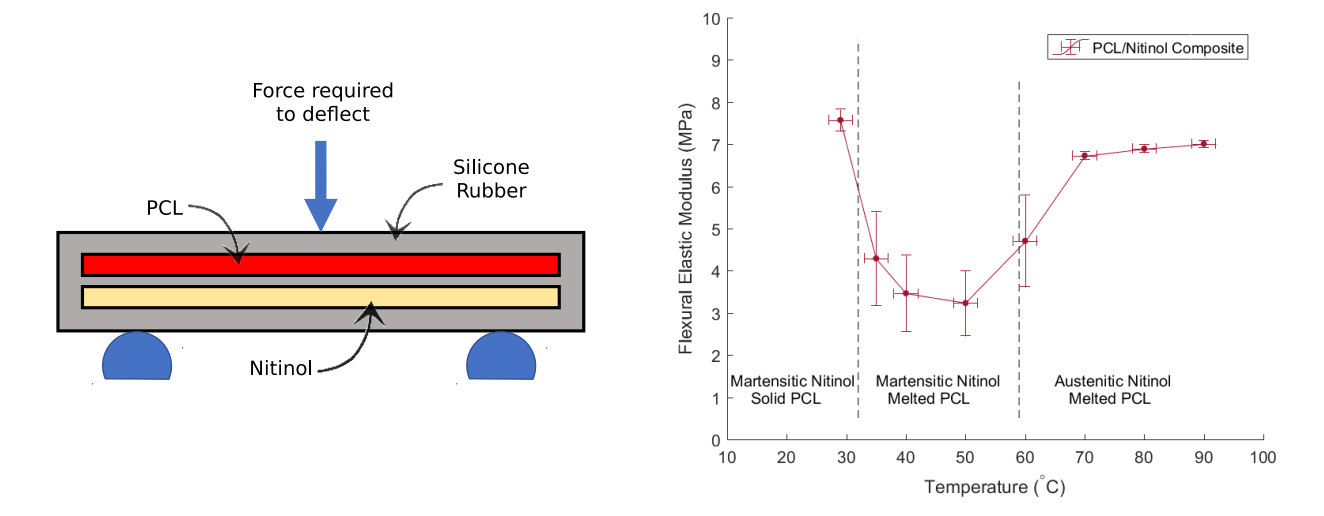


Figure 1. Three discrete stiffness regions achieved by composite of Nitinol and PCL rods encased in a silicone rubber matrix. The modulus values were calculated from force and deflection measurements obtained from 3-point bend tests conducted on the composite beam at each of the temperatures shown.

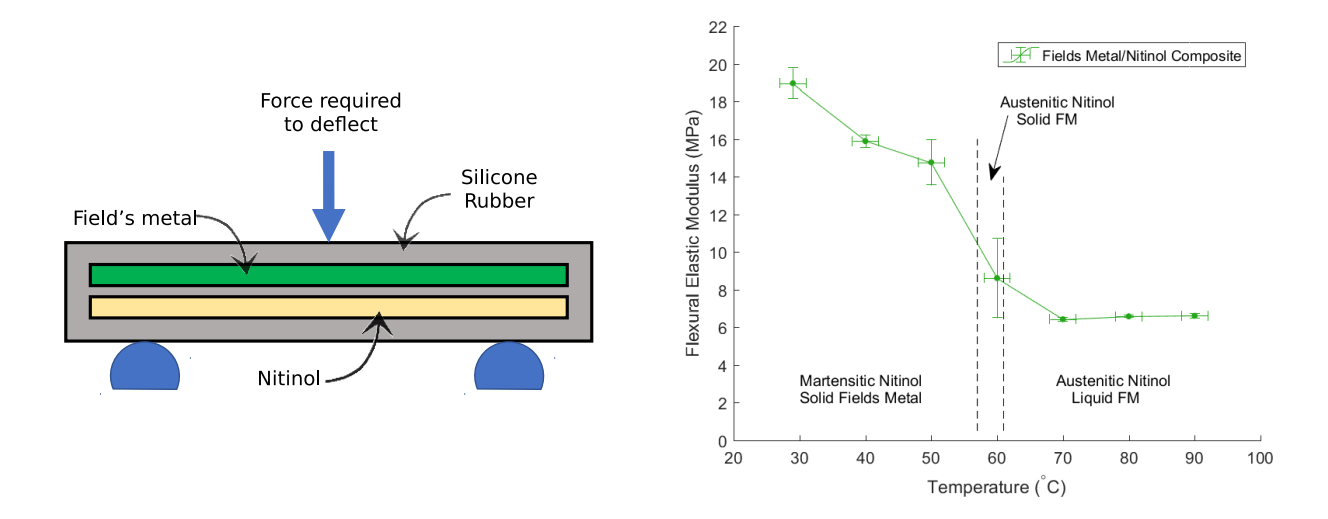


Figure 2. Two stiffness regions achieved by composite of Nitinol and Field's metal rods encased in a silicone rubber matrix. The modulus values were calculated from force and deflection measurements obtained from 3-point bend tests conducted on the composite beam at each of the temperatures shown. In this composite, a third stiffness level is not distinguishable because the constituent smart materials have nearly the same critical temperature.

driven robots with compliant backbones [20, 21, 22, 23]. More recently, origami approaches to generating compliant mechanisms have also been employed [24].

Other recent efforts which are similar to the proposed work involve the combination of heaters and low-melting point metals, but these methods are restricted to a very thin geometry and global heating [25, 26]. Other research using low melting point metals were focused on creating fabrics and threads with changeable stiffness [27, 28]. The work presented in this paper is a first step towards the long term goal of stiffness control in magnitude, directionality, and spatial resolution. The focus is no

longer just on the method of stiffening, as reviewed by Manti [29], but on how the compositing of multiple materials can result in multiple discrete stiffness levels within the same composite, as illustrated in figure 1 and figure 2.

# 2. Methods

Rods of Nitinol, PCL, and Fields metal (FM) are embedded in silicone rubber to form composite beams with variable stiffness due to the smart behavior of the constituent materials. 3-point bend tests are conducted on the composite beams and the individual

materials at temperatures spanning all three levels of discrete stiffness. Samples are held at constant temperature throughout each test which spans both the elastic and plastic range of deformation.

### 2.1. Smart Materials

As shown in table 1, each smart material used in this experiment exhibits a distinct change in stiffness at a specific critical temperature. This notable change in behavior can be explained by a change in microstructure or melting of the material. The critical temperatures and flexural modulus values listed in table 1 were extracted from data from the 3-point bend tests conducted on each material at constant temperature in this experiment. These values are evidenced by the data in figures 6, 7, and 8.

2.1.1. Nitinol Nitinol is a nickel-titanium alloy that exhibits the shape-memory effect. Above the austenite finish temperature, the nitinol becomes austenitic, increasing stiffness and making it resistant to deformation. Below the martensite finish temperature, this shape memory alloy transforms to a twinned martensite structure. Applying load to the material in its twinned martensite phase causes elastic deformation followed by de-twinning of the martensite. This detwinning process results in pseudo-plastic deformation up to 7% strain. When the material is reheated above its critical temperature, it returns to its initial shape as it transforms to austenite. This unique behavior is desirable for variable stiffness composites as it offers high stiffness at high temperatures where most materials become softer or melt. Chemically pickled shape memory Nitinol wire from Confluent Medical (P/N WSM007500000SE) was used for this experiment. This particular wire was observed to transform from martensite to austenite between 50 and 60 °C.

2.1.2. PCL Polycaprolactone (PCL) is a polyester that melts between 30-50 °C with a glass transition temperature of about 60 °C [30]. Unlike the instantaneous liquification of some materials, PCL softens gradually over a broad temperature range. It softens substantially before reaching its melting temperature, and even after melting completely, PCL remains extremely viscous. This transformation from a relatively rigid room temperature solid to a viscous melt at a slightly elevated temperature offers desirable behavior for varying stiffness at relatively low temperatures.

2.1.3. Field's metal Field's metal is a low melting-temperature eutectic alloy that melts uniformly at 62 °C. It is comprised of 51% indium, 32.5% bismuth,

and 16.5% tin by weight. Field's metal is relatively soft compared to other metals with an elastic modulus much lower than that of aluminum and other metals. It's low melting temperature lends itself to stiffness variability within a reasonable temperature range. Bismuth Indium Tin ingot Field's metal (stock number 46895) from Rotometals was used for this experiment.

# 2.2. Test sample preparation

To prepare the PCL rods for samples (b) and (e) from figure 3, six strands of 2.85mm diameter filament were cut to length, twisted around each other, and heated to a temperature just over 60 °C using a hand held heat gun. The heated strands were then rolled together by hand until the individual strands fused together, producing a uniform rod with a nominal diameter of 7.2mm.

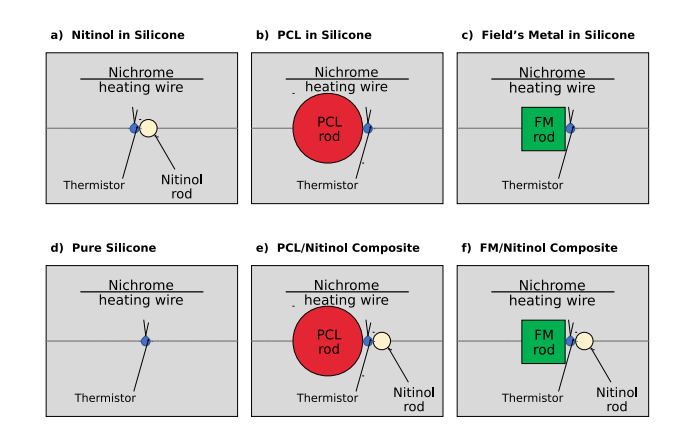


**Figure 3.** Cross-sectional diagram of composite samples fabricated for bend tests. Three of each sample were fabricated to verify repeatability between samples in the testing.

For the PCL/Nitinol composite, a PCL rod and an identical length of 1.91mm diameter Nitinol were positioned side-by-side in the center of an 18mm wide x 16.75mm high mold. An NTC 10K thermistor was situated snugly between the two rods. A Nichrome heating element formed into a serpentine pattern, was embedded near the rods to provide uniform Joule heating of the composite beam. The  $^{\rm TM}$  Dragon Skin 20 liquid silicone was cast in layers to ensure proper spacing of the rods, heating element, and thermistor within the mold.

The Field's metal rods for use in samples (c) and (f) from figure 3 were formed by melting the metal ingot and pouring the liquid metal into a 4.1mm x 4.1mm mold 3D printed with NinjaFlex brand filament. The process of compositing the FM/Nitinol sample was otherwise identical to the PCL/Nitinol composite sample previously described.

Nitinol, Field's metal, and PCL samples, intended for individual material testing, were encased in the

Table 1. Stiffness variability of individual smart materials.

Smart material	Critical temperature	Stiffness variability
Nitinol PCL Field's metal	$50\text{-}60^{\circ}\mathrm{C}$ martensite to austenite $30\text{-}50^{\circ}\mathrm{C}$ melting temperature range $62^{\circ}\mathrm{C}$ melting temperature	18 GPa to 65 GPa 200 MPa to 0 MPa 5 GPa to 0 GPa

silicone alone with the heating element and thermistor as shown in figure 3(a) to 3(c). These samples were created using the same methods described above for the PCL/Nitinol composite, but were enclosed in silicone without the Nitinol.

A pure silicone beam was also cast with no internal rods for determining the properties of the matrix material itself.

### 2.3. Test processes

3-point bend tests were conducted on individual materials (embedded in silicone) and composite beams using a Mark-10 Force Test Stand. As specified in the ISO standard for bend testing metallic materials, the equipment is fitted with polycarbonate supports with sufficient rigidity relative to the softer materials being tested [31]. The ASTM standard for bend testing plastic materials recommends a support span of 16 times the height of the testing specimen; the outer supports are spaced in conformance to the standard [32]. The polycarbonate loading nose attached to the load cell has a 10mm curvature radius to prevent the Nitinol from deforming at sharp, unrecoverable angles.

Load-deflection curves were obtained at 7 different temperatures for each beam: 29, 40, 50, 60, 70, 80, and 90 °C. The testing temperatures were chosen to capture the behavior of the materials in each stiffness region. Prior to testing, each sample was heated to the desired temperature by passing current through the heating element and monitoring the temperature with the embedded thermistor. The sample temperature was held constant through each test by toggling the heating element power supply on/off. Load and deflection data were collected simultaneously while the indenter was lowered at 5mm/s on the center of the specimen. Samples were tested up to 40 mm center deflection to investigate stiffness behavior under both plastic and elastic deformation at each of the test temperatures. As recommended by ASTM, toe compensation was made on the collected data to correct for the taking up of slack at the beginning of each test [32]. Tests were repeated with 3 identical samples under each set of conditions to verify repeatability. Samples that underwent permanent deformation were reset between tests by heating the materials up to 85°C and allowing them to cool to

melt and re-solidify any low melting temp materials or reset the shape of the shape memory Nitinol.

# 2.4. Smart composite finger

A PCL/Nitinol composite finger was also constructed to demonstrate the unique capabilities of robots constructed with composite smart materials. The finger was fabricated similarly to the PCL/Nitinol composite beam shown in figure 3, but notches in the top of the silicone were added to allow bending at two joint regions. A separate Nichrome heating element was embedded in each of the two joint segments. As seen in figure 4, a tendon was routed through sheathes in the silicone to minimize friction and prevent tearing of the silicone.



Figure 4. Relaxed configuration of PCL/Nitinol composite finger when tendon is slack.

By heating the joints individually to different temperatures, 9 different configurations should be achievable for any particular tendon force since each joint can exhibit 3 different stiffnesses as evidenced by figure 1. Whereas most robotic fingers would require separate tendons for each joint to control the relative joint angles, the smart composite finger should produce various joint angle combinations with a single tendon by using temperature to control the relative joint stiffnesses.

### 3. Results

Bend testing of the individual materials and composite beams revealed the stiffness variation and critical temperatures of each sample. The flexural elastic modulus is calculated from the equation

$$E = \frac{mL^3}{4wh^3} \tag{1}$$

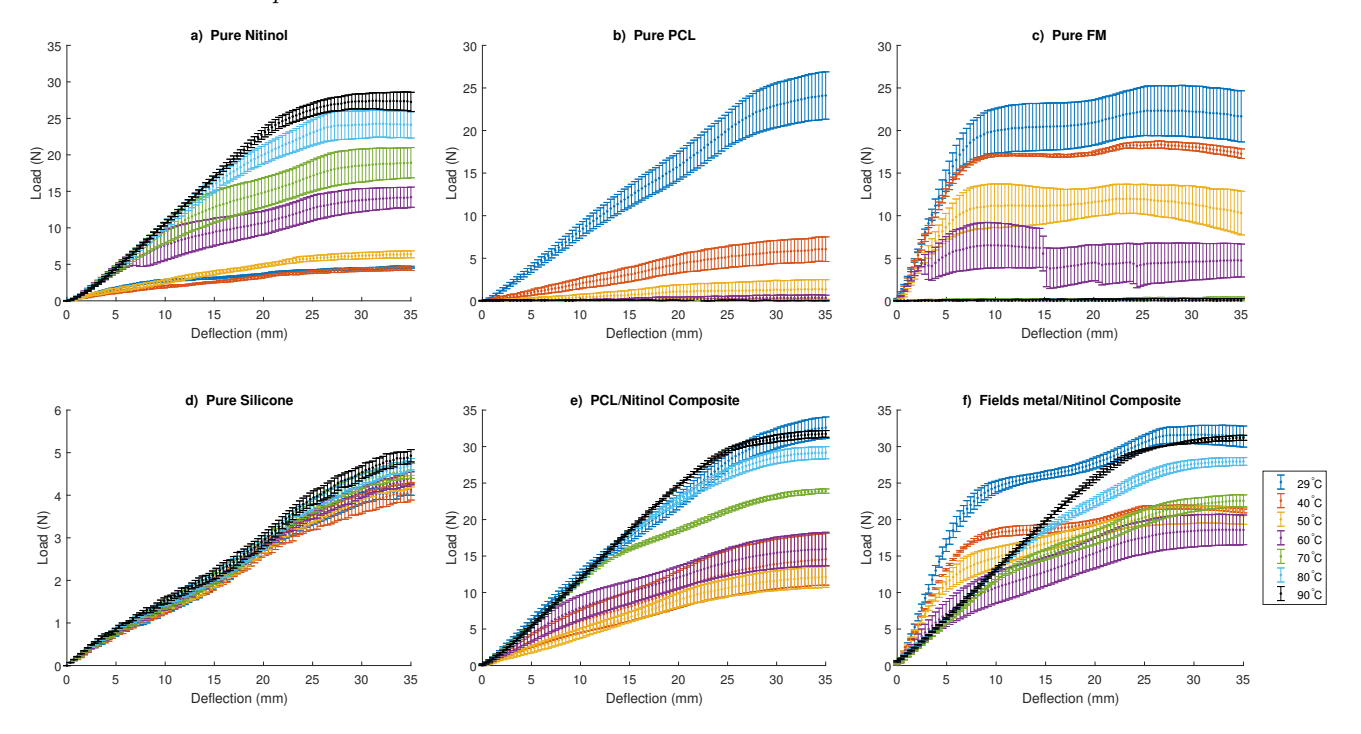


Figure 5. Load-deflection curves for each individual and composite sample. Vertical error bars represent repeatability error between 3 tests conducted at each temperature.

for rectangular beams, or

$$E = \frac{4mL^3}{3\pi d^4} \tag{2}$$

for beams with round cross sections [32]. In both Equations 1 and 2, m represents the slope of the initial linear region of the measured force-deflection curve; L is the support span and w, h, and d are the geometric dimensions of the specimens.

The load-deflection curves obtained from the constant temperature tests are plotted for each individual and composite material. These plots, shown in figure 5, are used to characterize the materials' behavior under both elastic and inelastic loading. The Nitinol, PCL, and Field's metal were all encased in silicone for testing to maintain their shape when tested above the melting points. However, we wish to characterize the behavior of the smart materials themselves, so the measured loads from the pure silicone sample were subtracted from the loads measured for the Nitinol, PCL, and Field's metal embedded in silicone to isolate the loads incurred by the smart materials themselves. This subtraction method relies on the assumption that the volume of silicone occupied by the smart material rods is negligible. In other words, the bending stiffness of the pure silicone beam is not significantly different than the bending stiffness of the silicone encasing the smart materials because the hollow channels occupied by the smart materials in the silicone are relatively narrow and are positioned along the nuetral axis. To verify this assumption, the bending inertia of the solid silicone beam and a silicone beam with hollow channels matching the dimensions of the encased smart material rods were calculated and compared. These inertia values differed by less than 2%, so this assumption should not significantly affect the results. The load-deflection curves shown in figures 5(a) to 5(c) show the loads incurred by the smart materials themselves, with the effects of the silicone matrix subtracted from the plotted results.

These results are converted to elastic modulus values using equations 1 and 2, where m is extracted from the load-deflection curves by evaluating slope of the initial, linear range of deformation. Figures 6, 9, 7, and 8 show the temperature dependence of the elastic modulus values of the individual materials. The temperature-dependent moduli of the composite beams are shown above in figures 1 and 2.

Vertical error bars in each of the plots represent repeatability error calculated as the standard deviation of the mean values from 3 identical tests conducted on separate samples. The thermistors used to measure temperature have a nominal random uncertainty of  $\pm 0.3\,^{\circ}\mathrm{C}$ ; however, additional uncertainty exists in these measurements due to the thermal gradient across the samples. The maximum thermal gradient across the width of the smart material rods was measured to be  $2\,^{\circ}\mathrm{C}$  when the samples were held at  $90\,^{\circ}\mathrm{C}$ . A much higher temperature gradient exists across the width of the entire silicone beam, but this gradient

is insignificant since the stiffness of the silicone does not change substantially with temperature. Thus, the uncertainties in the temperature measurements reflect both the accuracy of the thermistor readings and the temperature gradient across the smart material rods, resulting in a total uncertainty of  $\pm$  2.02°C in all temperature measurements. Deflection measurements have minimal uncertainty in the load-deflection data collected at constant temperature because zeroing the load cell and performing toe compensation removes any bias error from the data.

#### 3.1. Nitinol

As seen in figure 5(a), the force required to deflect the Nitinol varies significantly with temperature. The pseudo-elastic behavior is seen in the long linear portions of the curves from the 80 and 90 °C tests. The similarity between the 29, 40, and 50 °C curves suggests that the Nitinol has hardly begun to transition to austenite at 50 °C; this indicates that complete transformation occurs at a higher temperature. The flexural elastic modulus of the Nitinol shown in figure 6 exhibits two distinct levels of stiffness with a visible jump between the two levels at the transition from martensite to austenite between 50 and 60 °C.

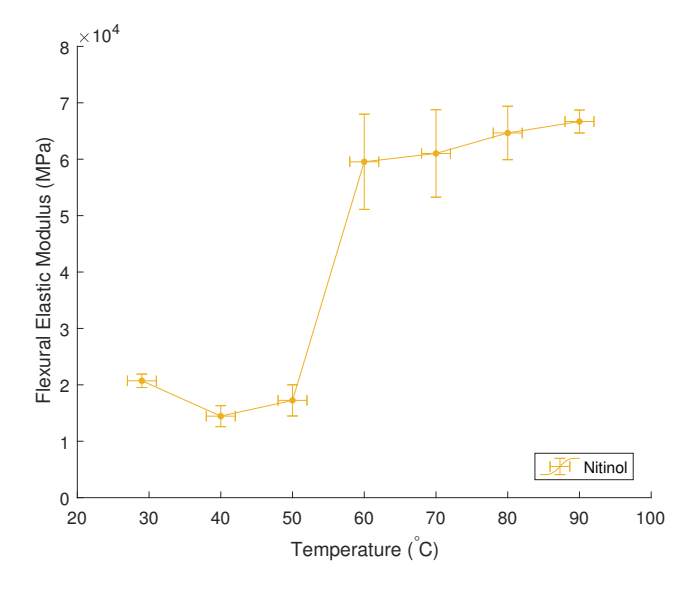


**Figure 6.** Flexural elastic modulus of pure Nitinol measured at a constant elastic deflection over a range of temperatures. The modulus values were obtained using the slopes of the load-deflection curves in figure 5(a).

### 3.2. PCL

The PCL bend tests were conducted on a PCL rod encased in silicone. The load measurements from the pure silicone tests in figure 5(d) are subtracted from the PCL/silicone load-deflection data to isolate the

load incurred by the PCL itself, shown in figure 5(b). The silicone load values can be subtracted directly without scaling since the pure silicone beam and the silicone encasing the PCL rod have equal dimensions. Repeatability error from the two sets of collected data are combined in quadrature to account for error propagated in this subtraction.

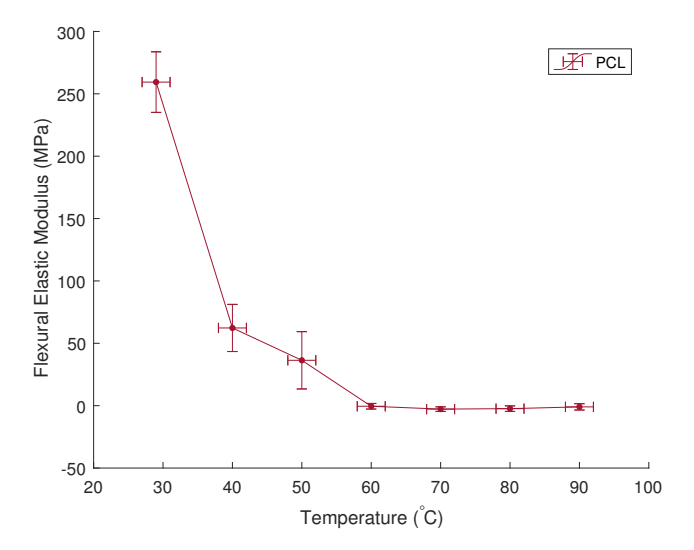


Figure 7. Measured flexural elastic modulus of pure PCL rod as a function of temperature. The modulus values were obtained using the slopes of the load-deflection curves in figure 5(b).

The PCL rod shows a drastic change in strength and stiffness between the 29 and 40 °C tests seen in figure 5(b). The elastic moduli shown in figure 7 show that the rod becomes essentially limp at temperatures beyond 50 °C, suggesting that the PCL melts gradually between about 30 and 50 °C. When heated beyond its melting temperature, the PCL turns into a viscous melt, thus the modulus platteaus at temperatures between 60 and 90 °C.

# 3.3. Field's metal

The Field's metal bend tests were conducted on a Field's metal rod encased in silicone since testing cannot be conducted on a material in its liquid state if it is not encased in a matrix material. Just as in the case of the PCL, the load measurements from the pure silicone load-deflection data, shown in figure 5(d) are subtracted from the Field's metal/silicone load data to isolate the load incurred by the Field's metal itself, shown in figure 5(c). Repeatability error from the two sets of collected data are again combined in quadrature.

A sharp melting point is expected from the Field's metal due to its eutectic nature. As seen in figure 8, the Field's metal shows some gradual decrease in overall strength when heated from 29 to  $60\,^{\circ}$ C, and a significant drop in stiffness when heated beyond its melting point  $(62\,^{\circ}$ C).

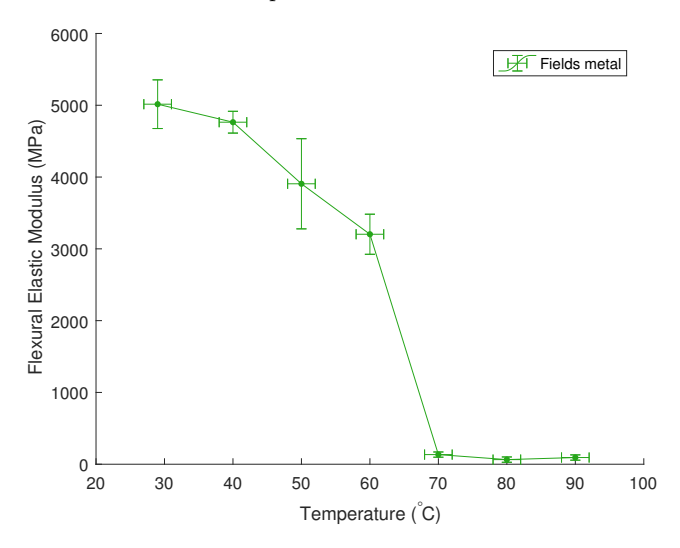


**Figure 8.** Measured flexural elastic modulus of pure Field's metal rod as a function of temperature. The modulus values were obtained using the slopes of the load-deflection curves in figure 5(c).

# 3.4. Silicone

The silicone rubber's contribution to the overall stiffness of the composite beams is minimal in comparison to the rigid smart materials, but its stiffness is analyzed experimentally nevertheless for the sake of improved accuracy. Figure 5(d) shows the load-deflection data from measurements taken at all 7 testing temperatures; the silicone's behavior is nearly identical at each of the temperatures.

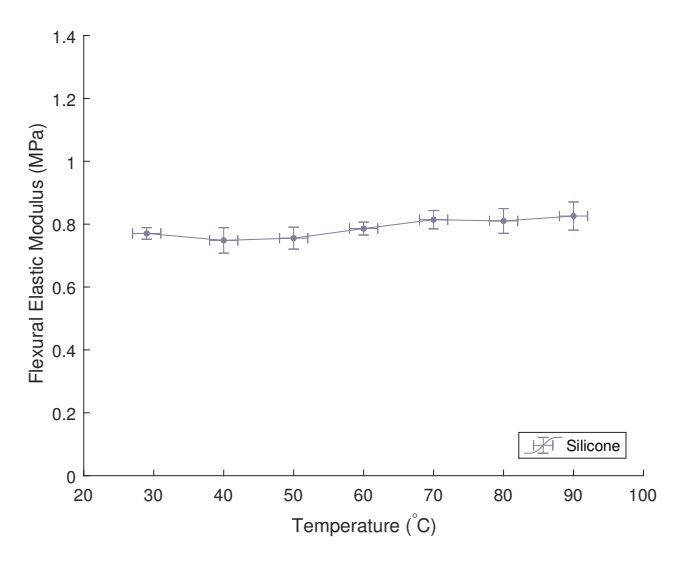
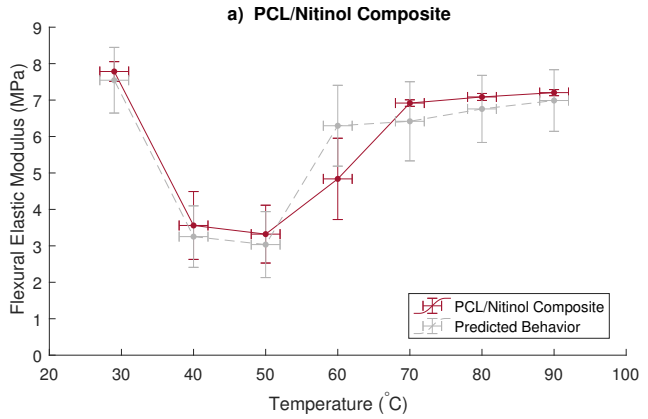


**Figure 9.** Measured flexural elastic modulus of pure silicone rubber as a function of temperature. The modulus values were obtained using the slopes of the load-deflection curves in figure 5(d).

The silicone serves primarily as a matrix for combining smart materials and does not exhibit smart behavior itself. In other words, the material properties of the silicone are not expected to change significantly with temperature. This lack of temperature-dependence in the stiffness is also evidenced by the plot in figure 9 which shows nearly constant elastic modulus across the range of temperatures.

# 3.5. PCL/Nitinol composite

The smart composite consisting of Nitinol and PCL rods in the silicone matrix offers desirable stiffness variability. The PCL rod provides high stiffness at low temperatures while the Nitinol rod exhibits high stiffness at high temperatures. At mid-range temperatures, both materials provide minimal rigidity to the composite, causing very low stiffness at temperatures around 40 to 50 °C. The beam stiffness is characterized by its flexural elastic modulus calculated from the slopes of the load-deflection curves from figure 5(e).



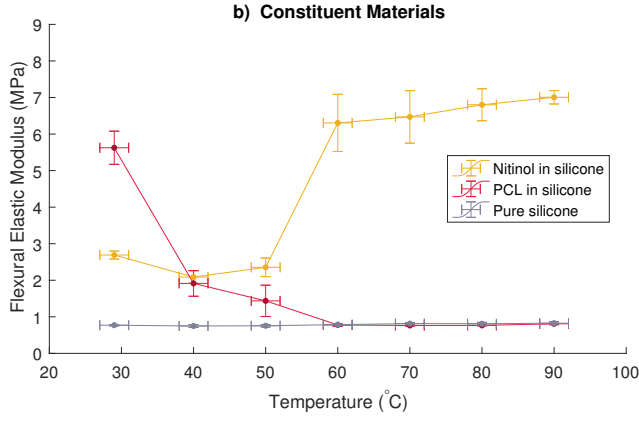


Figure 10. Measured flexural elastic modulus of PCL/Nitinol Composite and constituent materials as a function of temperature. The dashed gray curve in (a) shows the predicted modulus of the composite based on the sum of the individual material moduli.

As seen in figures 1 and 10, three discrete stiffness levels are observed between temperatures of 29 and 90 °C. This unique stiffness variation across the range

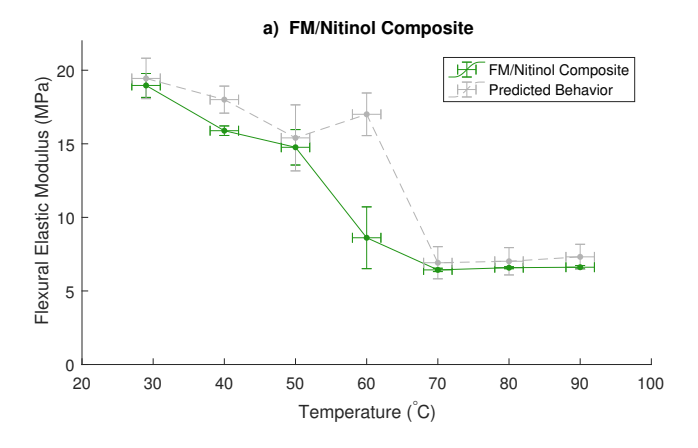
of temperatures is due to the smart behavior of its constituent materials. Theoretically, the sum of the loads incurred by the pure PCL, Nitinol, and silicone should match the measured load of the composite beam at any temperature. The modulus values in figure 10(a) and (b) were all calculated from equation 1 using the geometric dimensions of the silicone for w and h. Since the values of w and h were the same for each sample, the modulus of the PCL/Nitinol composite should line up with the sum of the moduli of the constituent materials. The shape of the curve in figure 10(a) does indeed match nearly identically the summation of the modulus curves for the constituent materials in figure 10(b).

The highest stiffness for the PCL/Nitinol composite beam is achieved at temperatures below about 30 °C, where the Nitinol is martensitic and the PCL remains solid. The modulus in at 29 °C reaches up to 7.8  $\pm$  0.3 MPa. The stiffness reaches a minimum of 3.3  $\pm$  0.8 MPa around 50 °C when the composite becomes flexible as the PCL melts. The Nitinol remains martensitic in this region, allowing large deformation as the microstructure transforms from twinned to detwinned martensite. The medium stiffness range occurs between 70 and 90 °C with an average modulus of 7.1  $\pm$  0.1 MPa where the PCL is melted but the Nitinol transforms to austenite.

A unique twisting behavior was observed in the testing of the PCL/Nitinol composite above 60 °C;, the composite twisted under the applied load of the bend test. At low temperatures, the parallel rods resist torsion, but above 60 °C, the PCL melts and provides no resistance to torsion in the composite beam. When applied to bulk materials, this feature could provide directional stability upon localized melting of specific PCL members.

# 3.6. Field's metal/Nitinol composite

The combination of the smart behavior of Nitinol and Field's metal in the silicone rubber matrix results in a composite beam with unique, temperature-dependent properties. The Nitinol again provides the composite with high stiffness at high temperatures. Similar to the PCL, the Field's metal also offers high stiffness at low temperatures, but the Field's metal melts at a higher temperature than the PCL. Because the Field's metal has a higher melting point than the PCL, the 3 distinct stiffness regions are not distinguishable in figures 2 and 11(a). The reason for this indistinct stiffness region at mid-range temperatures is explained by the behavior of the constituent materials shown in figure 11(b). As the Field's metal begins to soften and melt, the Nitinol simultaneously transitions to austenite which counteracts the stiffness change of the Field's metal as it melts. In the case of the PCL/Nitinol composite, the PCL melted before the Nitinol began its phase transformation, which resulted in a low stiffness region at mid-range temperatures. For the Field's metal/Nitinol composite, however, the smart behavior of the constituent materials is activated at roughly the same temperature, so only 2 distinct stiffness regions are visible in figures 2 and 11(a).



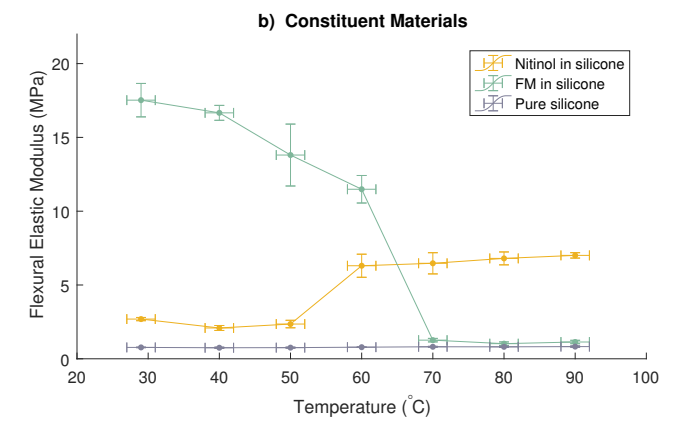


Figure 11. Measured flexural elastic modulus of FM/Nitinol Composite and constituent materials as a function of temperature. The dashed gray curve in (a) shows the predicted modulus of the composite based on the sum of the individual material moduli.

At room temperature (29 °C), the combination of the martensitic Nitinol and solid Field's metal produces a stiffness of 19.0  $\pm$  0.8 MPa. As the composite is heated, the Field's metal begins to soften and weaken the beam while the Nitinol begins simultaneously transforming to austenite, causing a gradual decline in stiffness. The composite reaches a minimum modulus of  $6.4 \pm 0.1$  MPa at 70 °C. Beyond this point, the Field's metal remains melted and the Nitinol is completely austenitic, so the stiffness platteaus and remains relatively constant with further heating.

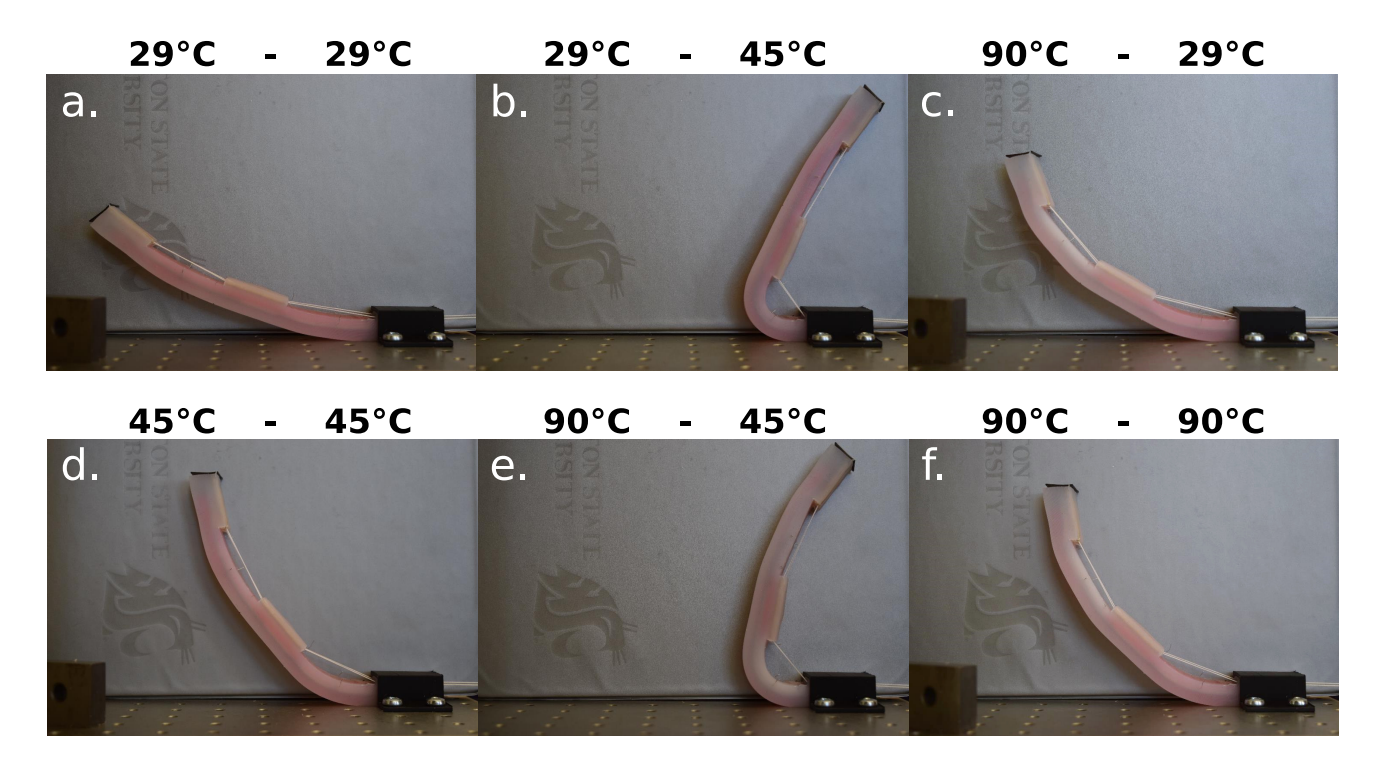


Figure 12. Six different finger configurations achieved with a single tendon. Different combinations of joint temperatures enabled 6 different configurations with the application of the same 20N tendon force in each scenario.

**Table 2.** Joint temperatures for 9 configurations achieved by 2-joint PCL/Nitinol composite finger actuated by the same 20N tendon force. Note that configurations g, h, and i are mirrored versions of the configurations marked with an  $^*$ .

Config- uration	Distal Joint		Proximal Joint		Tendon
	Temp	Stiffness	Temp	Stiffness	Force
a	29 °C	high	29 °C	high	20N
$b^*$	$29^{\circ}\mathrm{C}$	high	$45^{\circ}\mathrm{C}$	low	20N
$c^*$	$90^{\circ}\mathrm{C}$	medium	$29^{\circ}\mathrm{C}$	high	20N
d	$45^{\circ}\mathrm{C}$	low	$45^{\circ}\mathrm{C}$	low	20N
$e^*$	$90^{\circ}\mathrm{C}$	medium	$45^{\circ}\mathrm{C}$	low	20N
f	$90^{\circ}\mathrm{C}$	medium	$90^{\circ}\mathrm{C}$	medium	20N
g	$45^{\circ}\mathrm{C}$	low	$29^{\circ}\mathrm{C}$	high	20N
h	$29^{\circ}\mathrm{C}$	high	$90^{\circ}\mathrm{C}$	medium	20N
i	$45^{\circ}\mathrm{C}$	low	$90^{\circ}\mathrm{C}$	medium	20N

# 3.7. Smart composite finger

As shown in figure 12, the PCL/Nitinol composite finger proved capable of forming 6 different configurations with a single tendon tensioned at 20N. The PCL/Nitinol composite bend test results from figure 10(a) showed that the composite can exhibit 3 different stiffness levels between 29 and 90 °C: high stiffness at low temperatures, low stiffness at mid-range temperatures, and medium-high stiffness at high temperatures. By heating the finger joints to various combinations of

temperatures in different stiffness regions, the shape of the finger can be precisely controlled. Table 2 shows the joint temperatures for all 9 configurations possible with a 20N tendon force. Configurations g, h, and i are not shown in figure 12 because they are simply mirrored versions of configurations b, c, and e.

### 4. Discussion

Ultimately, the PCL/Nitinol composite exhibited 3 different stiffness levels at temperatures between 29 and 90 °C, and the Field's metal/Nitinol composite showed a jump between two stiffness levels at about 60 °C. Due to the smart behavior of the constituent materials, these different stiffness levels may be activated with a simple temperature stimulus. In this experiment, a thin resistance wire was used to supply Joule heating to the composites, but other heating methods could be used that may offer more uniform heating. Methods for heat dispersion should also be explored as cycling time is a concern among most shape memory alloys and other thermally activated systems.

In order to develop an effective system for controlling composite smart materials, it is necessary to develop an accurate model for the composite beam stiffness. Due to the smart behavior of each component and their inelastic behavior under large loads, the composite beam stiffness is a complicated function of both temperature and applied load. The recoverable strain limit is a factor that limits the usability of smart material composites for robotics applications. The PCL and Field's metal can endure unlimited strain because they may be melted and re-solidified to reset any permanent deformation. Thus, the composite stiffness relies on not only the current strain, but also on the configuration at which the PCL or Field's metal was last allowed to solidify. The shape memory effect of the Nitinol allows it to recover from any deformation up to 7% strain when heated above its transformation temperature. However, when the Nitinol is austenitic, deformation beyond the elastic limit is unrecoverable and thus limits the load the composite is capable of exerting.

The melting and re-solidifying of the low melting temperature materials (PCL and Fields metal) further complicates the model, but we seek to develop a model that characterizes the behavior of the two composite beams under all temperatures and applied loads.

In this experiment, tests were conducted on composite beams comprised of rods with one specific size and shape. However, customization of the stiffness in each temperature region may be achieved by modifying the geometry of the individual rods. This will alter the bending inertia of the individual materials and allow the magnitude of each discrete stiffness region to be customized to suit the relevant application. The temperature stimuli can also be shifted slightly by changing material compositions and alloying elements. For example, the Field's metal/Nitinol composite only showed two stiffness regions because the critical temperature of the Nitinol was too close to the melting point of the Field's metal to allow an intermediate stiffness region. However, by slightly altering the alloy composition of the Field's metal, the melting point can be easily adjusted. There also exist other low melting point materials that may be useful for incorporating in smart composite robotics.

The PCL/Nitinol composite exhibited three different stiffness regions as we had anticipated. However, the high stiffness and medium stiffness levels were very similar, almost to the extent that the high-low-medium stiffness sequence might be considered a high-low-high sequence. Depending on the application, a more diverse range of stiffness levels may be desired. The relative stiffness levels can be easily tuned by simply altering the thickness ratio of the smart materials used. For example, by using a thinner Nitinol rod without changing the dimensions of the PCL, the composite would exhibit a more distinct medium stiffness level at high temperatures.

# 5. Conclusion

Composite beam samples were constructed with combinations of PCL/Nitinol and Field's metal/Nitinol rods positioned in parallel within a silicone matrix. The resulting composite stiffness was evidenced through 3point bend tests conducted on the composite beams and their constituent materials at 7 different temperatures between 29 and 90 °C. Three discrete stiffness levels were observed in the behavior of the PCL/Nitinol composite beams. Twisting behavior was also observed in the case of the PCL/Nitinol composite as the PCL melted and allowed rotation about the Nitinol rod. The Field's metal/Nitinol composite beam exhibited only tow stiffness levels between 29 and 90 °C because the melting of the Field's metal and the phase transformation of the Nitinol ocurred at nearly the same temperature. Heating of the PCL/Nitinol composite resulted in a high, low, medium stiffness sequence. The Field's metal/Nitinol composite exhibited high stiffness at low temperatures and lower stiffness at higher temperatures. By including different smart materials and modifying the relative thicknesses of the constituent materials, the stiffness levels and temperature ranges can be finely tuned to suit a variety of applications.

Characterizing the stiffness as a function of temperature for composite smart materials and their constituent materials is a substantial step toward developing adept soft robotic materials. From these results we found a visible correlation between the composite stiffness and the stiffness of each constituent material at any given temperature. Thus, by selecting appropriate smart materials, smart composites with numerous stiffness levels at different temperatures may be designed, and the stiffness of the resulting composites may be predicted through a simple weighted summation of the component stiffnesses.

As demonstrated by the smart composite finger, compositing multiple smart materials in parallel within a robotic member could enable highly dexterous manipulation with minimal complexity. Nine different configurations were achieved with single tendon by selectively heating the joints to activate different stiffness levels. By including more smart materials, more stiffness levels could be achieved, enabling more precise control.

Applications for smart composite materials extend beyond the realm of simple robotic fingers to meet design requirements in applications ranging from wearable devices to co-robotic environments and inhome health care. Further research will explore the effects of extending these smart material composites into 3 dimensions and thereby enabling highly intelligent manipulation.

# Acknowledgments

This research was funded by the National Science Foundations National Robotics Initiative Award 1734117. The authors declare no conflict of interest. The founding sponsors had no role in the design of the study; in the collection, analyses, or interpretation of data; in the writing of the manuscript, or in the decision to publish the results.

#### References

- [1] Schmidt-Nielsen K 1997 Animal physiology: adaptation and environment (Cambridge University Press)
- [2] Kier W and Smith K 1985 Zoological Journal of the Linnean Society 83 307 – 324
- [3] Horchler A D, Kandhari A, Daltorio K A, Moses K C, Andersen K B, Bunnelle H, Kershaw J, Tavel W H, Bachmann R J, Chiel H J and Quinn R D 2015 Wormlike robotic locomotion with a compliant modular mesh Biomimetic and Biohybrid Systems ed Wilson S P, Verschure P F, Mura A and Prescott T J (Cham: Springer International Publishing) pp 26–37
- [4] Ijspeert A J 2014 Science 346 196-203 ISSN 0036-8075 (Preprint http://science.sciencemag.org/content/ 346/6206/196.full.pdf) URL http://science. sciencemag.org/content/346/6206/196
- [5] Palagi S, G Mark A, Reigh S, Melde K, Qiu T, Zeng H, Parmeggiani C, Martella D, sanchez castillo A, Kapernaum N, Giesselmann F, Wiersma D, Lauga E and Fischer P 2016 Nature Materials advance online publication
- [6] Mazzolai B and Cianchetti M 2016 Science Robotics  ${f 1}$
- [7] Tonietti G, Schiavi R and Bicchi A 2005 Design and control of a variable stiffness actuator for safe and fast physical human/robot interaction Robotics and Automation, 2005. ICRA 2005. Proceedings of the 2005 IEEE International Conference on (IEEE) pp 526–531
- [8] Schiavi R, Grioli G, Sen S and Bicchi A 2008 Vsa-ii: a novel prototype of variable stiffness actuator for safe and performing robots interacting with humans Robotics and Automation, 2008. ICRA 2008. IEEE International Conference on (IEEE) pp 2171–2176
- [9] Tsagarakis N G, Sardellitti I and Caldwell D G 2011 A new variable stiffness actuator (compact-vsa): Design and modelling Intelligent Robots and Systems (IROS), 2011 IEEE/RSJ International Conference on (IEEE) pp 378–383
- [10] Tagliamonte N L, Sergi F, Accoto D, Carpino G and Guglielmelli E 2012 Mechatronics 22 1187–1203
- [11] Vanderborght B, Albu-Schäffer A, Bicchi A, Burdet E, Caldwell D G, Carloni R, Catalano M, Eiberger O, Friedl W, Ganesh G et al. 2013 Robotics and autonomous systems 61 1601–1614
- [12] Paul C, Roberts J W, Lipson H and Cuevas F V 2005 Gait production in a tensegrity based robot ICAR'05. Proceedings., 12th International Conference on Advanced Robotics, 2005. (IEEE) pp 216–222
- [13] Shibata M, Saijyo F and Hirai S 2009 Crawling by body deformation of tensegrity structure robots Robotics and Automation, 2009. ICRA'09. IEEE International Conference on (IEEE) pp 4375–4380
- [14] Iscen A, Agogino A, SunSpiral V and Tumer K 2013 Controlling tensegrity robots through evolution Proceedings of the 15th annual conference on Genetic and evolutionary computation (ACM) pp 1293–1300
- [15] Paul C, Valero-Cuevas F J and Lipson H 2006 IEEE Transactions on Robotics 22 944–957
- [16] Majidi C 2014 Soft Robotics 1 5–11
- [17] Daerden F and Lefeber D 2002 European journal of mechanical and environmental engineering 47 11–21
- [18] Trivedi D, Rahn C D, Kier W M and Walker I D 2008 Applied Bionics and Biomechanics 5 99–117
- [19] Beyl P, Van Damme M, Van Ham R, Vanderborght B and Lefeber D 2014 Mechatronics, IEEE/ASME Transactions on 19 1046–1056
- [20] Li C and Rahn C D 2002 Journal of Mechanical Design 124 265–271
- [21] Hannan M W and Walker I D 2003 Journal of Robotic Systems 20 45–63

- [22] Calisti M, Giorelli M, Levy G, Mazzolai B, Hochner B, Laschi C and Dario P 2011 Bioinspiration & biomimetics 6 036002
- [23] Laschi C, Cianchetti M, Mazzolai B, Margheri L, Follador M and Dario P 2012 Advanced Robotics 26 709–727
- [24] Vander Hoff E, Jeong D and Lee K 2014 Origamibot-i: A thread-actuated origami robot for manipulation and locomotion 2014 IEEE/RSJ International Conference on Intelligent Robots and Systems (IEEE) pp 1421–1426
- [25] Shan W, Lu T and Majidi C 2013 Smart Materials and Structures 22 085005
- [26] Wang W, Rodrigue H and Ahn S H 2015 Composites Part B: Engineering 78 507–514
- [27] Chenal T P, Case J C, Paik J and Kramer R K 2014 Variable stiffness fabrics with embedded shape memory materials for wearable applications Intelligent Robots and Systems (IROS 2014), 2014 IEEE/RSJ International Conference on (IEEE) pp 2827–2831
- [28] Shan W, Diller S, Tutcuoglu A and Majidi C 2015 Smart Materials and Structures 24 065001
- [29] Manti M, Cacucciolo V and Cianchetti M 2016 IEEE Robotics & Automation Magazine 23 93–106
- [30] Pcl low temperature filament natural 2.85mm https://filaments.ca/products/pcl-low-temperature-filament-natural-2-85mm
- [31] 2005 Metallic materials Bend test Standard International Organization for Standardization Geneva, CH see also URL http://allaboutmetallurgy.com/wp/wp-content/ uploads/2016/12/ISO-7438.pdf
- [32] 2003 Standard Test Methods for Flexural Properties of Unreinforced and Reinforced Plastics and Electrical Insulating Materials Standard ATSM International see also URL http://mahshahr.aut.ac.ir/lib/exe/fetch. php?media=labs-astmd-790.pdf